Supporting Information for "Widespread initiation, reactivation, and acceleration of landslides in the northern California Coast Ranges due to extreme rainfall"

Alexander L. Handwerger[1], Eric J. Fielding[1], Mong-Han Huang[2], Georgina L Bennett[3], Cunren Liang[4], and William H. Schulz[5]

[1]Jet Propulsion Laboratory, California Institute of Technology, Pasadena, CA, USA.
[2]Department of Geology, University of Maryland, College Park, MD, USA.
[3]School of Environmental Sciences, University of East Anglia, Norwich, UK.
[4]California Institute of Technology, Seismological Laboratory, Pasadena, CA, USA.
[5]U.S. Geological Survey, Denver, CO, USA.

Contents

Additional Supporting Information (Files uploaded separately)

1. Tables S1 to S2

Introduction

This supporting information provides additional figures and tables.

Corresponding author: Alexander L. Handwerger, alexander.handwerger@jpl.nasa.gov

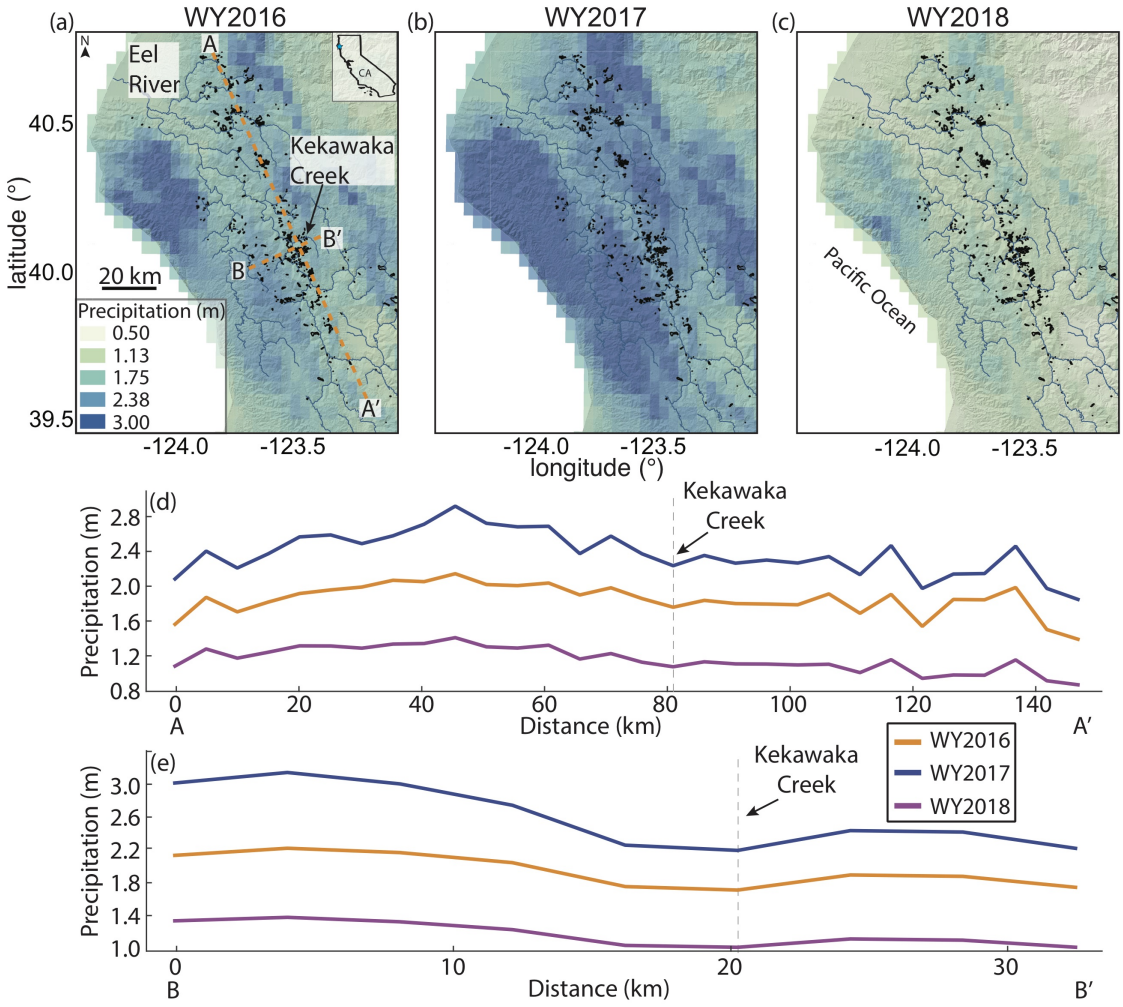

Figure S1. Precipitation maps for northern California Coast Ranges. (a,b,c) cumulative precipitation for the 2016, 2017, and 2018 water years draped over a hillshade of the topography. Black polygons show mapped slow-moving landslides from this study and from previously published inventories (Bennett et al., 2016a; Mackey and Roering, 2011; Handwerger et al., 2015). Thin blue lines show major rivers and tributaries. (d,e) Cumulative precipitation profiles plotted by water year from A to A' and B to B'. Precipitation data from PRISM (http://prism.oregonstate.edu/) and digital elevation model from TanDEM-X.

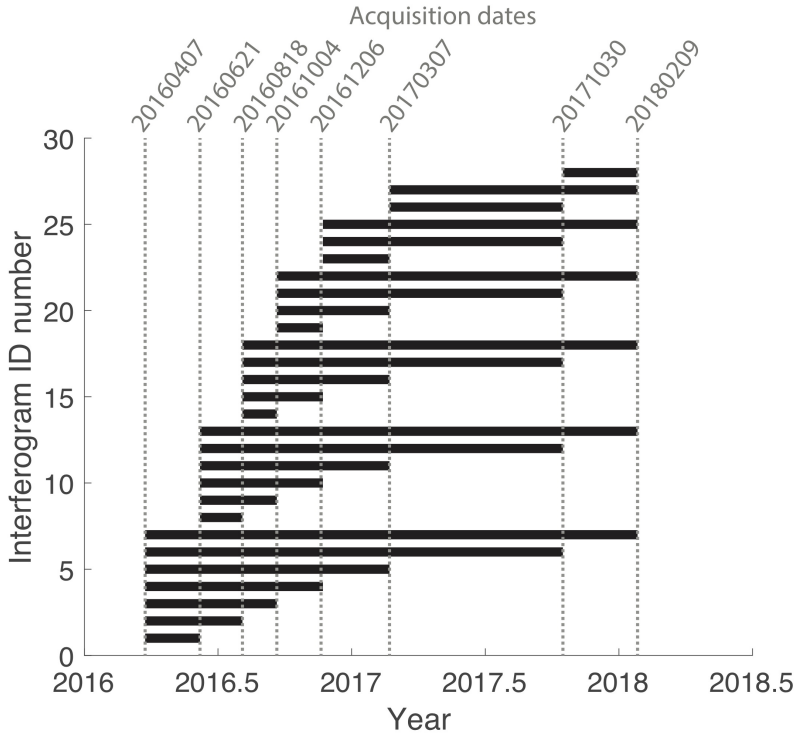

Figure S2. Temporal distribution of interferograms and pixel offset tracking pairs. Graphical depiction of the 28 interferogram/pixel offset tracking pairs for a single flight path. The vertical dashed lines show the dates of each of the eight data-collection flights. Because there are four flight paths, the number of pairs available for analysis is 112.

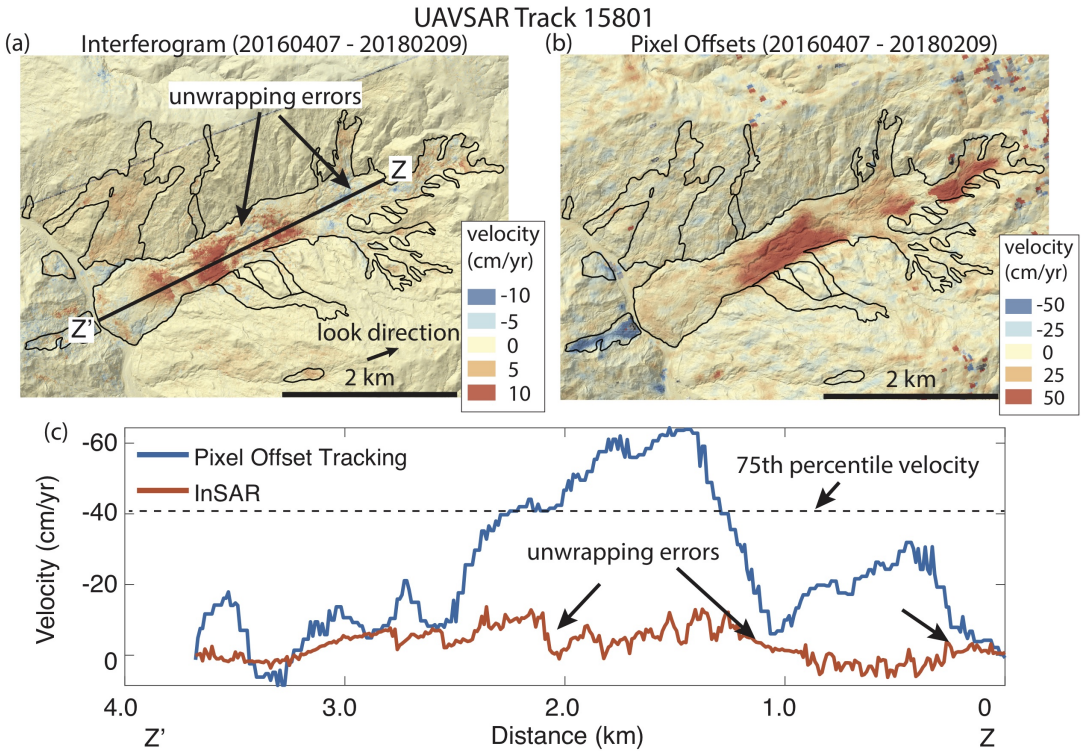

Figure S3. Example of unwrapping errors at the Boulder Creek landslide. (a) Long time-period interferogram velocity map with unwrapping errors draped over a hillshade of the topography. (b) Long time-period pixel offset tracking velocity map draped over a hillshade of the topography. (c) Profiles down the center of the landslide axis from Z to Z'. The dashed black line shows the 75th percentile velocity value for the pixel offset tracking profile. In Section 4.2 of the main text, we define the 75th percentile value as the characteristic landslide velocity. We highlight this value here for illustrative purposes (i.e. to show how the 75th percentile value compares to overall spatial variations in landslide velocity). Digital elevation model from OpenTopography (http://www.opentopography.org).

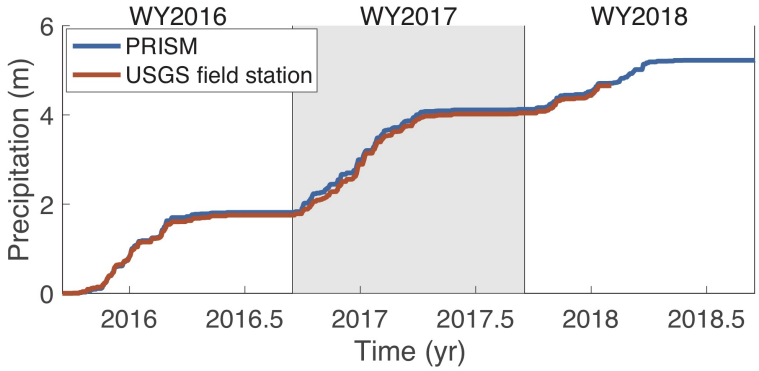

Figure S4. Precipitation time series. Cumulative precipitation measured at a USGS field station on the Two Towers landslide, Kekawaka Creek, CA (Schulz et al., 2018b; see location in Figure 4) and calculated by PRISM (http://prism.oregonstate.edu/). We find generally good agreement between the PRISM and ground based data. See Figure 3a for location of field station.

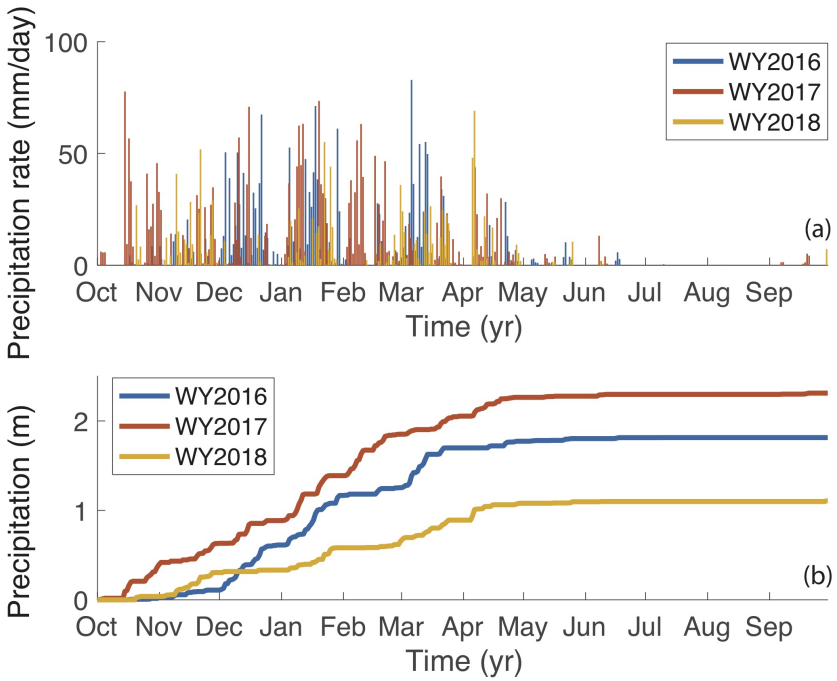

Figure S5. Precipitation time series for 3 water years condensed into a single year time period. (a) Precipitation rate and (b) cumulative precipitation for each water year in our study period. Seasonal precipitation displays similar first-order pattern each season with large differences in the magnitude of cumulative precipitation. Precipitation data are from PRISM (http://prism.oregonstate.edu/).

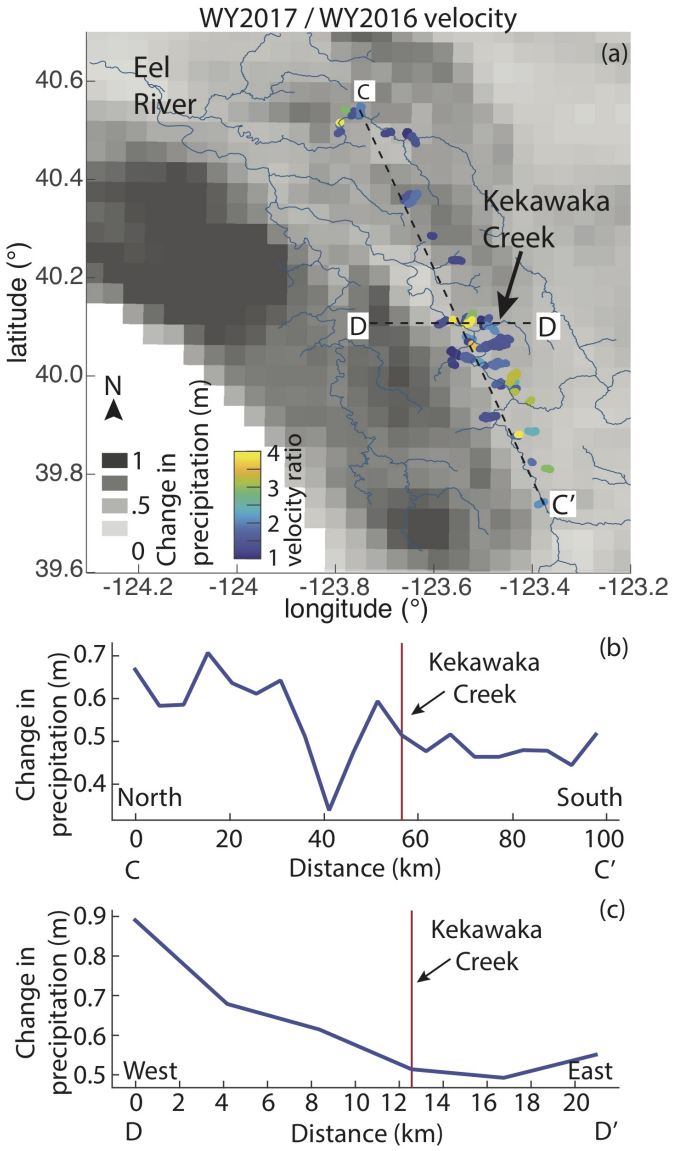

Figure S6. Velocity and precipitation changes between WY2017 and WY2016. (a) Velocity ratio, defined as the velocity between March – October, 2017 (WY2017) divided by the velocity between April – October, 2016 (WY2017) for each landslide draped over change in precipitation map, defined as WY2017 total precipitation minus WY2016 total precipitation. (b,c) Change in total precipitation between WY2017 and WY2016 across North to South (C to C') and West to East (D to D') profiles. The largest change in velocity occurs for the group of landslides in the SE which has the smallest change in precipitation. This suggests that landslide geometry is the strongest control on changes in landslide motion from year to year (Figure 9). Precipitation data from PRISM (http://prism.oregonstate.edu/).

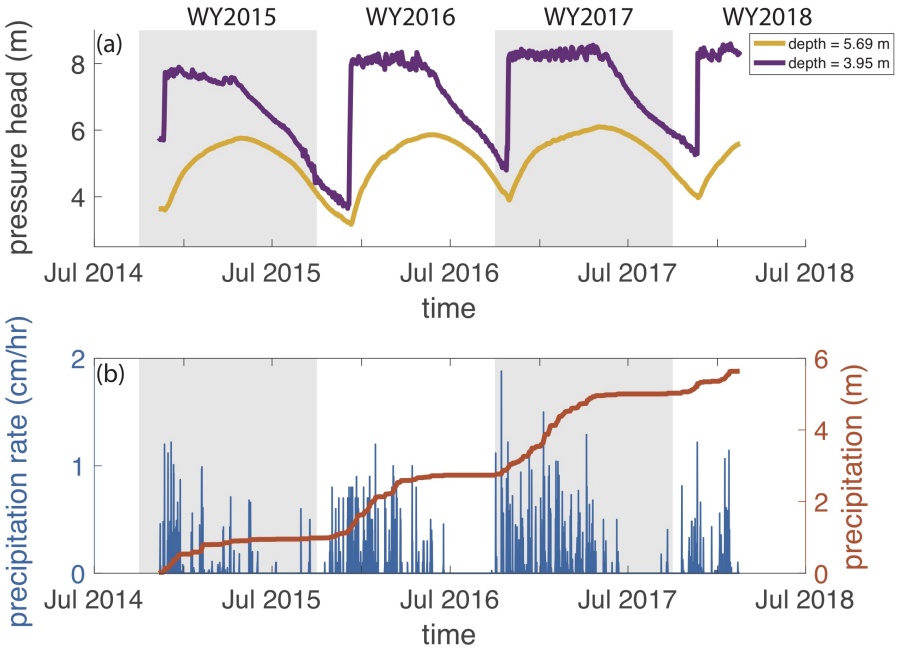

Figure S7. Pore pressure head and rainfall measured at Two Towers landslide, Kekawakwa Creek, California. Pore pressure head is measured at two depths below the ground surface at the same location. Data are from Schulz et al. (2018b). See Figure 4 for landslide location.

Table S1. List of interferogram and pixel offset tracking pairs. Columns correspond to the pair number, acquisition date of the master image, acquisition date of the slave image, the change in time between master and slave images. The same pairs were processed for all 4 UAVSAR flight tracks. Figure S2 also shows the interferogram pairs.

Table S2. Landslide inventory statistics. Columns correspond to area (m^2), length (m), width (m), mean slope angle (deg), slope angle standard deviation (deg), max slope angle (deg), min slope angle (deg), and mean elevation (m). Data are provided for the WY2016, WY2017, WY2018 landslides, landslides that were only active in WY2017, and landslides that were moving during the full study period.